TOWARDS COMPLETE SPECTROSCOPY IN RAPIDLY ROTATING NUCLEI*

B. HERSKIND, S. LEONI, T. DOSSING, G.B. HAGEMANN
The Niels Bohr Institute, University of Copenhagen
Blegdamsvej 17, 2100 Copenhagen, Denmark

P. BOSETTI, A. BRACCO, S. FRATTINI, E. VIGEZZI
Dipartimento di Fisica, Universitá di Milano
Via Celoria 16, 20133 Milano, Italy

M. MATSUO
Yukawa Institute for Theoretical Physics, Kyoto University
Kyoto, Japan

(Received January 23, 1995)

The progress in γ-spectroscopy is discussed with special emphasis on the transition region in excitation energy, from the rather well known cold nuclei characterized by regular rotational motion built on specific single particle configurations with well defined quantum numbers, to the region above 800 keV in heat energy, where the rotational motion is damped, as a result of a spreading of the rotational transition strength, due to residual interactions acting between the close lying bands. A general analysis scheme is advocated, aiming at a more direct comparison between the experimental results and theoretical models to give a more complete picture of nuclear structure going from cold to warm nuclei. A simulation model for describing the rotational and statistical decay of high spin states has been developed based on microscopically calculated energies and the spreading of rotational transition strength due to residual interactions. The calculations predict that *scars* of regular rotational motion may be found at excitation energies as high as 2 MeV above yrast, far into the region characterized by damped rotational motion. Traces of this new phenomenon are identified and studied in the experimental spectra from high spin states in rare earth nuclei. A prominent example of isolated structures in the quasi-continuum region are bands built on high-K quantum numbers. Recent results from a fluctuation analysis of counts in low-K and high-K configurations in ^{163}Er are discussed, and indicate that states in the quasi-continuum feeding high-K bands are different from states feeding the low-K bands.

PACS numbers: 21.60.-n, 21.10.Re

---

* Presented at the XXIX Zakopane School of Physics, Zakopane, Poland, September 5–14, 1994.

1. Introduction

The tremendous progress in γ-spectroscopy in these years, inspired by the access to more and more sensitive γ-detector arrays both in US (HERA $\rightarrow$ GAMMASPHERE) and in Europe (TESSA, OSIRIS, NORDBALL $\rightarrow$ GASP, EUROGAM $\rightarrow$ EUROBALL III), will soon make it possible to resolve the complete quantum spectrum up to the limits of discrete spectroscopy. The limits are imposed by rotational damping [1] in heat energy (the energy above yrast), and by fast fission in angular momentum space. Detailed knowledge, towards a complete understanding of the dynamics of the well defined quantal system, the nucleus, is thereby at reach. In general, we would like to learn much more about the nuclear structure response to the fictive forces induced by rapid rotation, or more specifically, the breaking of time reversal symmetries in the intrinsic frame, deviation from the mean field description and the residual interactions, the quenching of the static pairing and the role of dynamic pair correlations at the highest spins, the role of higher multipoles in surface interactions, exotic shapes and shape fluctuations to mention some of the most obvious which come into mind. Most of this may be learned from the study of the lowest lying well resolved discrete states at high spin.

As shown previously [2] by use of The Fluctuation Analysis Method (FAM), analyzing fluctuation of counts in the 2-D $E_{\gamma 1} \cdot E_{\gamma 2}$ spectra from the decay of high spin states, the regular rotational bands accessible to discrete spectroscopy are limited to $\approx$ 10 rotational bands on the average for each parity and signature (π, α), until damping of the rotational motion becomes dominating at $U_0 \approx 800$ keV. Above this borderline energy, with the exception of high-K- and strongly deformed (SD) bands, we may have to be satisfied with analysis methods and theoretical comparisons of the statistical type, such as analyzing fluctuations of counts, by extracting variances, co-variances and auto-correlations from the experimental spectra, [3], or studying the rotational correlations in higher fold coincidence spectra in both the experimental spectra and corresponding simulations.

Most recently the so-called *scars* of the typical rotational band structures known from the discrete region have been identified, at heat energies as high as 2 MeV. The rotational correlated *scars* were first found in realistic cranking calculations on multi-particle, multi-hole states including residual 2-body interactions [4], in an attempt to understand inconsistencies in the spectrum shapes, and soon after indications found in the experimental observations [5]. These exciting observations and the new possibilities they open for tracing rotationally correlated structures in the spectra from the quasi-continuum, will be discussed in more detail in Section 4.

More generally speaking, it is time now to aim for a *complete analysis scheme*, in which an overall comparison between the accurately deter-

mined experimental observables, E_γ, N_γ, I, τ, fluctuations, and corresponding quantities calculated within the different models can be performed in a flexible and interactive way. We try to illustrate this ambitious goal in a schematic form in Fig. 1.

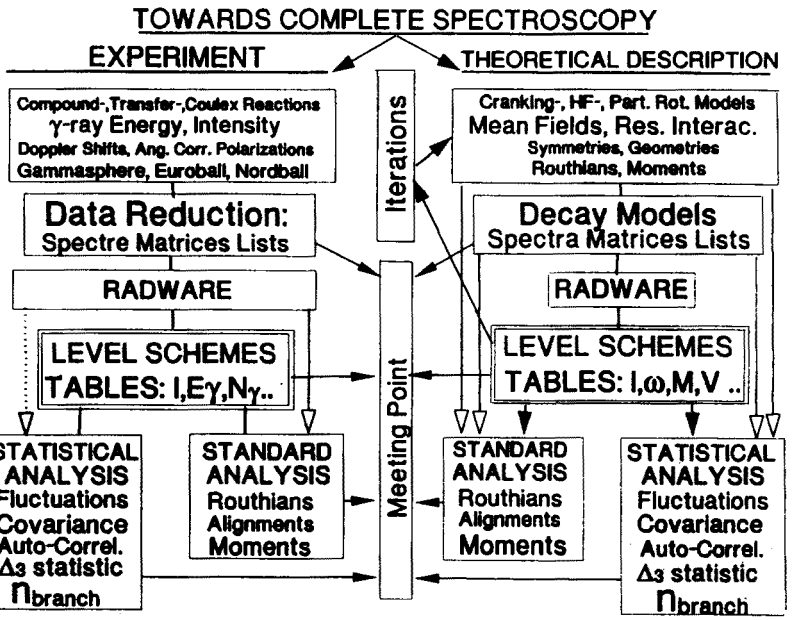

Fig. 1. The principles of the "complete" analysis scheme discussed in the text are shown.

2. Simulation of rotational spectra

One of the new ingredients in this scheme would be a decay model, which can accept appropriate inputs from different theoretical models and output parameters and spectra which can be directly compared, to the experimental observables. With this in mind, a new simulation model, *Montestella* of the Monte Carlo type, has been developed very recently [6, 7]. The experimental observables are calculated, by assuming a statistical decay process of competing E1($\Delta I = 0$), E1($\Delta I = 1$), E2($\Delta I = 2$), from the entry states formed in the reactions to the final states at the yrast line, via a decaying flow of γ-rays through microscopically calculated levels. The distribution of transition strength, for each of the decay steps is deduced from band mixing calculations and inserted as a table look-up routine. The quantal structure of the states, and the transition strengths of the decay branches given in the look-up tables are initially based on the cranking+band mixing model

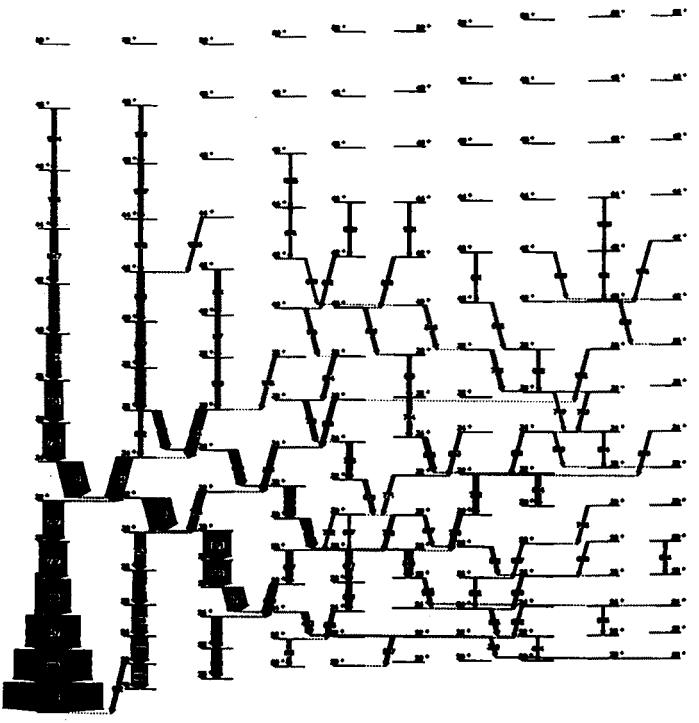

Fig. 2. The calculated level scheme for ^{168}Yb for the lowest 10 levels of $(\pi, \alpha) = (+, 0)$ from spin 20–60 $\hbar$. The 112 E2 transitions found to be above 0.5 % of the total intensity going into ^{168}Yb are shown.

MIXLAB by Matsuo *et al.* [8]. These calculations without pairing are made for the spin range $20 < I < 60\hbar$ only.

When the residual interaction and band mixing are included one sees how the rotational transitions from each level I branch out to many levels at the next step $I - 2$ as predicted by the damping model. The first 400 levels of each spin, parity and signature (I, π, α), which is shown to be almost free of truncation problems are used as input, with calculated branchings between all possible states, and with extrapolations to higher excitation energies according to expectations of average properties from the damping model. One of the first and most simple comparisons to make within the analysis scheme described above would be to deduce both experimental and theoretical level schemes, and compare both energies of the levels and intensities of the transitions. By the help of RADWARE [9] these are easy to produce in very flexible forms. Other sensitive comparisons may be made by the standard analysis techniques, comparing Routhians (energies in a rotating frame), alignments of the single particle orbits, lifetimes

and moments. As the level statistics improve in the coming years, the statistical analysis techniques almost exclusively used to-day for the study of the quasi-continuum become meaningful, and may in fact be very useful in discrete line spectroscopy also, for tracing and studying specific configurations which have feeding characteristics different from the main flow, such as superdeformed- or high-K bands [10].

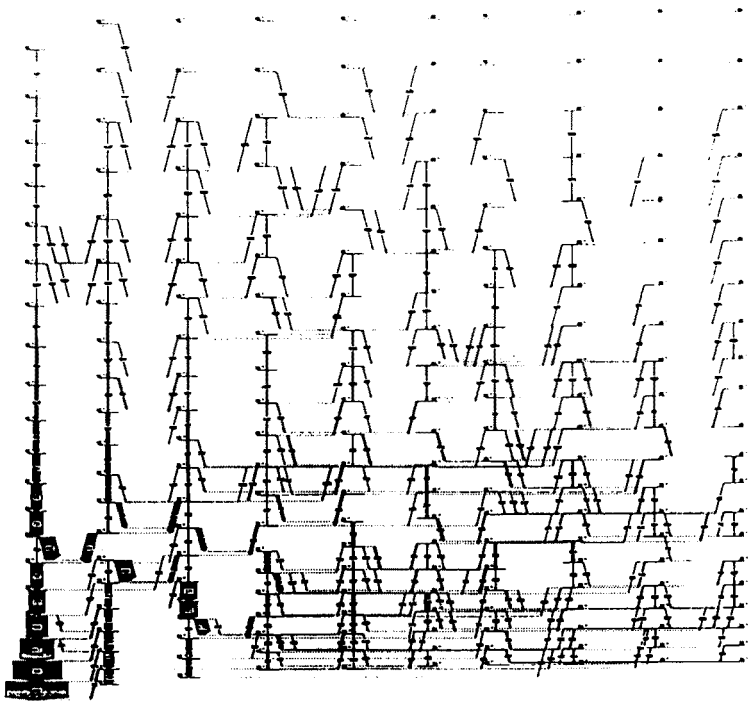

Fig. 3. The calculated level scheme for ^{168}Yb for the lowest 10 levels of $(\pi, \alpha) = (+, 0)$. 361 rotational E2 transitions with an intensity larger than $4 * 10^{-5}$ are shown.

Theoretical level schemes, with intensity of the individual transitions indicated by the thickness of the arrows are shown in Figs 2 and 3 for the lowest lying 10 bands of $(\pi, \alpha) = (+, 0)$ for $I \geq 20\hbar$, and for 2 different intensity limits. It is clearly seen from these two figures, how the spectrum becomes much more complex, for increasing sensitivity (lower limit for the weakest transition to be observed) of the experiment. The spectrum shown in Fig. 3 would roughly correspond to the "discrete structures" one may expect to observe in ^{168}Yb with $(\pi, \alpha) = (+, 0)$, below the on-set of rotational damping, using a powerful array as the advanced EUROGAM II array

with a total photopeak efficiency of $\Omega\varepsilon_{\mathbf{peak}} = 9\%$. Please note the significant branching between the many close lying states even for the lowest lying bands shown here, the type of branchings which so far is only very rarely observed. With the sensitivity of NORDBALL type instruments, $\Omega\varepsilon_{\mathbf{peak}} \approx 1$ %, one may rather expect to see the spectra shown in Fig. 2, with much

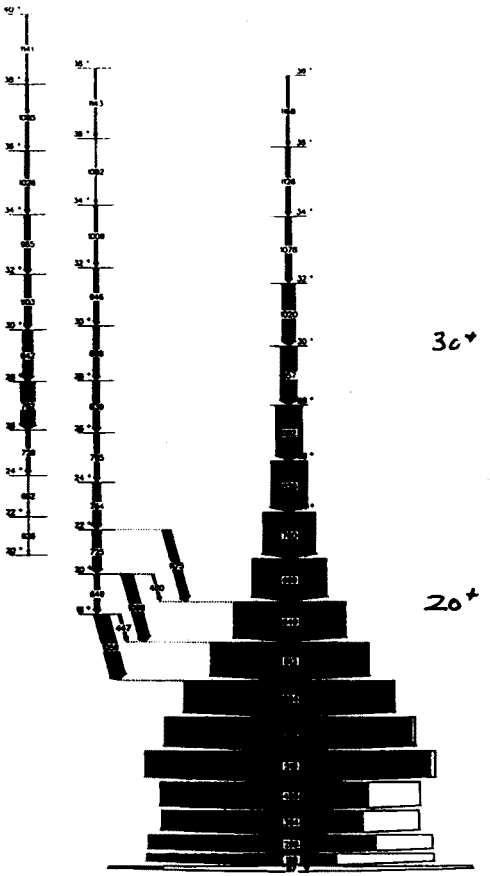

Fig. 4. The experimental level scheme for ^{168}Yb for the observed levels of $(\pi, \alpha) = (+, 0)$. The bands are from a recent analysis of EUROGAM I data [11].

less branching because the sensitivity limit is too poor for the branchings to be observed. It is also noted that in Fig. 2, only 3 regular rotational cascades are observed, (shown with vertical arrows) together with bits and pieces of the other bands. The level structure of the corresponding $(\pi, \alpha) = (+, 0)$ taken from a recent study of ^{168}Yb using the EUROGAM I array, [11] is shown in Fig. 4 for comparison. It is interesting to note that only 3 ro-

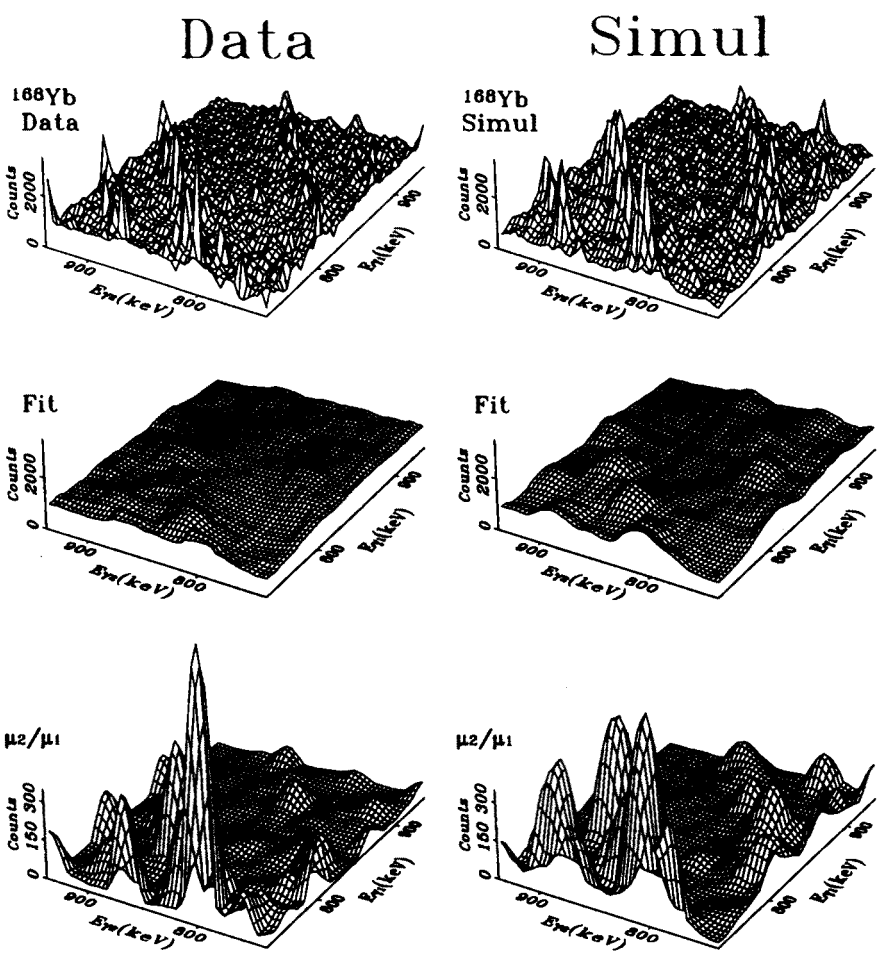

Fig. 5. Comparison between experimental data on ^{168}Yb and simulations by the Montestella code based on cranking+band-mixing calculation on ^{168}Yb .

tational bands with many consecutive transitions above $I = 20\hbar$ has been found so far, in general agreement with the simulated spectra in Fig. 2 and 3. The band crossings at real high spin have not been found yet in this nucleus, as those predicted in the most strongly populated bands shown to the left in Fig. 3, around $I = 50$. On the other hand, such crossings are also hidden in Fig. 2. After the full GAMMASPHERE and EUROBALL III come into operation, within a few years, the tools would be available to find a significant part of the predicted branchings at least for the strongly populated bands. If they are not found then it would be even more interesting, indeed.

The primary goal of the simulation was to be able to describe the overall spectrum-shape observed in the experiments, realizing that only a very small

fraction of the intensity in these spectra from the high spin region is present in resolvable peaks. Figure 5 shows examples from a comparable study of ^{168}Yb , with the data taken from a EUROGAM I experiment [12]. To make the comparison most realistic, the resolution of the experiment has been folded into the simulated spectra. Section of intensity spectra from the (E_γ = 850 keV, I $\approx$ 30) region are compared in the top of the figure, and similar spectra from a fluctuation analysis [12] are shown in the lower part. The ridge-valley structures are clearly well reproduced by the fluctuation analysis. In the more sensitive μ_2/μ_1 spectra even backbends and "scars" can be observed and compared in the valley.

It is anticipated, that the Montestella simulation model will be extended to accept several sets of levels in a multi-barrier scheme, to be able to simulate f. ex. the feeding and decay of superdeformed bands as discussed earlier [13], but here based on microscopically calculated levels [14], such that a fluctuation analysis on the superdeformed continuum can be made and compared to data. In "the complete analysis scheme" it should become possible also later to adjust the matrix elements which are most sensitive to the experimental observables by an interactive iterative procedure. In this way one may study the important differences between the model under investigation and the experimental data in a sensitive way.

The decay model is also a very useful tool to develop and investigate new analysis techniques, for the study of the rather unknown territory, *e.g.* the quasi-continuum. Here we shall only show an instructive example, to illustrate the importance of the residual two-body interactions, in describing the part of the 2-D $E_{\gamma 1} \cdot E_{\gamma 2}$ spectrum originating only from the lowest 40 levels of each (π, α). The 8 2-D $E_{\gamma 1} \cdot E_{\gamma 2}$ spectra shown in Fig. 6 are calculated for a specific spin sequence $(I = 42) \rightarrow (I = 38) \rightarrow (I = 38)$ assuming, no 2-body interaction (6a, 6e), a Surface Delta Interaction (SDI) of standard strength (6b, 6f) [15], SDI with half strength (6c, 6g), or SDI with double strength (6d, 6h). The lower 4 spectra 6a–6d shows the distribution of coincidence transitions for the lowest 10 levels of each (π, α), while the top 4 spectra (6e–6h) similarly shows the distribution for the lowest 40 states.

It is clearly seen how the transition energies in this restricted decay of the 4×10 and 4×40 configurations are completely correlated displaying the difference in alignment Δi, and the corresponding change in the collective spin $-\Delta R$ of the configurations which in all cases must add up to the same total spin, $I = (i + R) \propto (E_{\gamma 1} + E_{\gamma 2})$, if no interaction is applied. It also illustrate how the decay become very strongly fragmented when a residual two-body Surface Delta Interaction (SDI) is included in the diagonalization of the Hamiltonian, and how it depends on the interaction strength. However, we would like here especially to point to the correlated structure of

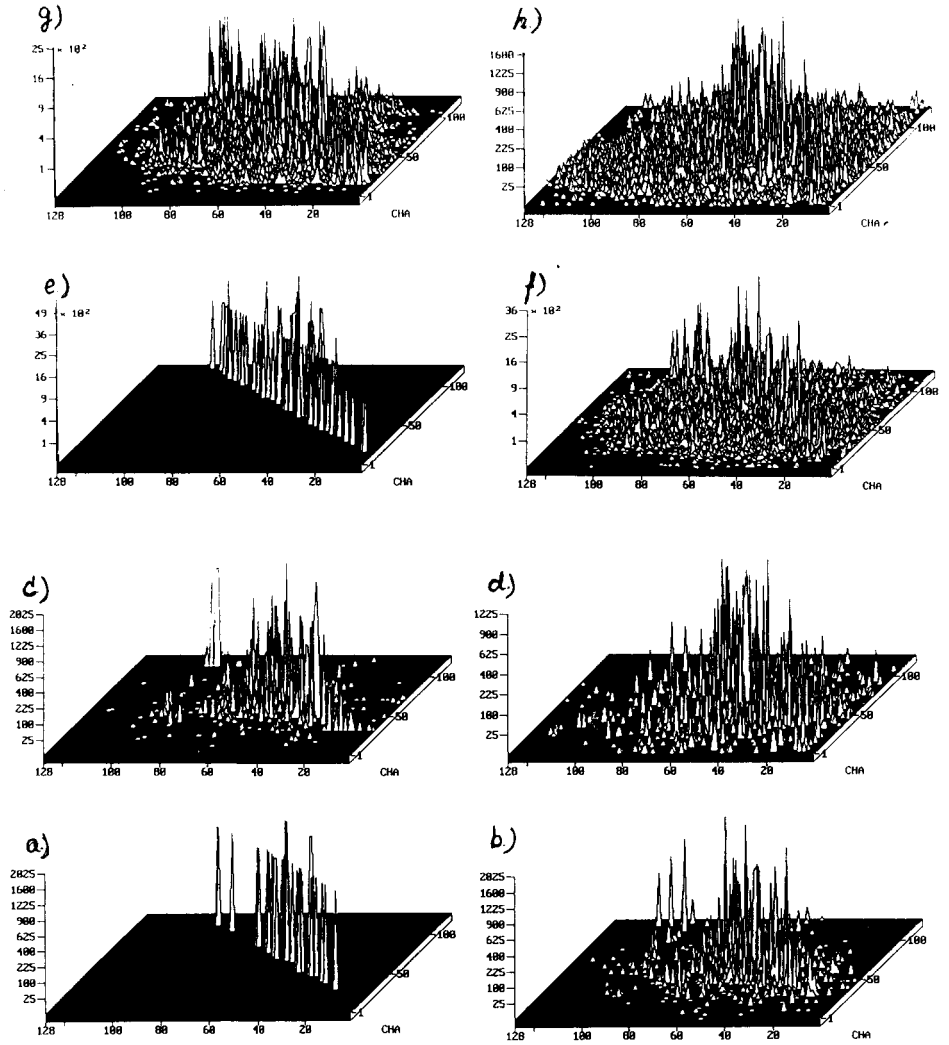

Fig. 6. Calculated spectra for a selected spin sequence $(I = 42) \rightarrow (I = 40) \rightarrow (I = 38)$ assuming, no 2-body interaction (6a, 6e), a Surface Delta Interaction (SDI) of standard strength (6b, 6f), SDI with half strength (6c, 6g), or SDI with double strength (6d, 6h). The lower 4 spectra 6a–6f show the distribution of coincidences for transitions between the lowest 10 levels of each (π, α) for $I = 40\hbar$). The 4 spectra (6e–6h) show the distribution for the lowest 40 states of each (π, α). The scale of γ-ray transition energies starts at a bias of 600 keV and cover a range of 512 keV with 4 keV/Channel.

sharp peaks at ridge positions parallel to the diagonal $E_{\gamma 1} = E_{\gamma 2}$ which are rather similar to the ridge seen with no-interaction, although with a much larger spread in the direction perpendicular to the diagonal $E_{\gamma 1} = E_{\gamma 2}$,

corresponding to changes in the moment of inertia $\mathcal{J}^{(2)}$, even for the 10 lowest states. This new correlated phenomenon which we name *scars* will be discussed in more detail in session 4.

3. γ-Ray Spectroscopy on ^{163}Er

With NORDBALL in its present configuration, we can approach the goal of complete spectroscopy on regular rotational bands reasonably well, in the spin region up to I $\approx 30\hbar$, where the bands in the low region of excitation energy are populated rather strongly, however with only a few E2 cross band branchings. Good frontline examples from NORDBALL are the study of ^{177}Re by Bark *et al.* identifying 30 rotational band structures [16], and ^{164}Yb by Nordlund *et al.*, finding 13 band structures in this even nucleus, but with several interesting examples of E2 branchings between different configurations. Also many E1's and M1's as well as 2 examples of M2 transitions are found [17]. In both cases the data are compared to detailed *ultimate cranking calculations*, in the intermediate spin region where pairing still is important.

We would like here to show another good example of modern discrete γ-ray spectroscopy, taken from an experiment made at the multi-detector array GA.SP, in Legnaro. This is of particular interest to us because the analysis shows for the first time, 4 different observations of E2 branchings caused by band mixing, in both low-K and high-K bands with both positive and negative parities, sometimes resulting in several cross band transitions of E2 type, all in the same nucleus, ^{163}Er. These types of branching are expected to be more and more dominating with increasing excitation energy, as discussed above and illustrated in Figs 2 and 3.

The GA.SP array consists of 40 Compton suppressed Ge detectors, surrounding an inner ball of 80 BGO crystals. It was used to measure γ-rays following the ^{18}O + ^{150}Nd reaction with a beam E_{beam} = 87 MeV on a 700μg/cm^2 target. Gates on the sum energy and fold spectra from the BGO inner-ball allowed a rather good separation of the contributions from the ^{162}Er, ^{163}Er and ^{164}Er reaction channels, with a final statistics of 2.9, 2.5 and 1.3 $\times$ 10^9 unfolded triple events, respectively. Figure 8 displays a part of the band structure of ^{163}Er with excitation energy as function of spin from the deduced level scheme [20], separated into positive parity- to the left and negative parity bands to the right. Note especially the observation of 3 high-K bands and one [505]11/2$^-$ configuration with long decay sequences isolated at rather high heat energy, extending into the region where the low-K bands are expected to be strongly mixed and rotational damped. The

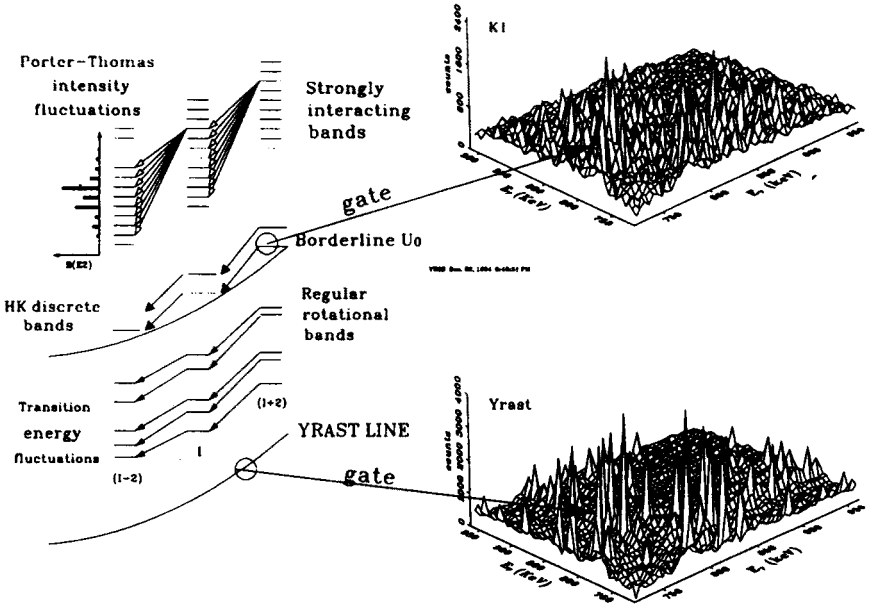

Fig. 7. In the bottom of this figure a section of a yrast gated $\gamma - \gamma$ spectrum of ^{163}Er is shown. A ridge-valley structure, coming from the cold region of regular rotational motion, is clearly visible and riding on a continuous distribution coming from the region of rotational damping that most cleanly can be found in the valley along the diagonal. Also shown in the upper part of the figure is how the same section looks like when gated by transitions in a high-K band, (K1), lying more than 1 MeV above the yrast line, in the region of damped motion for low-k states.

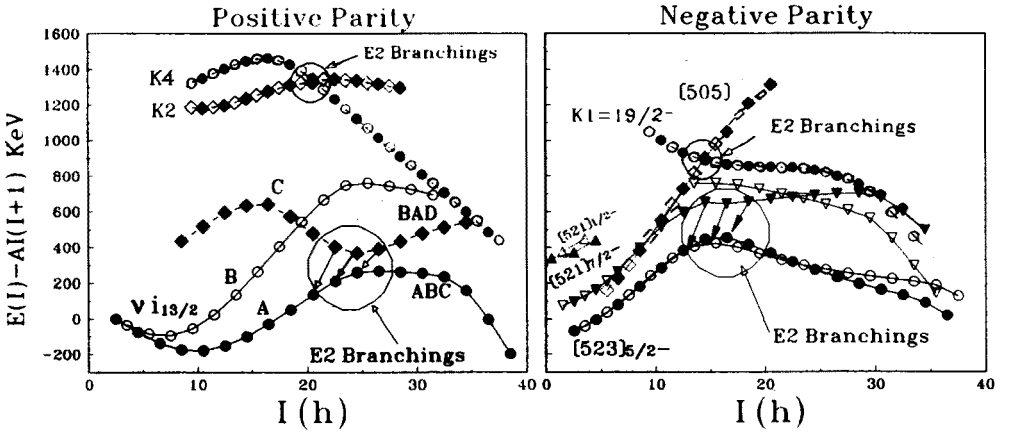

Fig. 8. Excitation energy versus spin for the three known high-K bands as labeled, and for the most intense low K configurations, selected for the study of the configuration dependence of $N^{(2)}_{\rm path}$. The bands are separated into positive (left) and negative (right) parities. The plotted energies are given relative to the rotational energy of a rigid body with $\mathcal{J} = 63.3\hbar^2$ MeV^{-1}.

interesting crossing regions where E2 branchings have been observed are marked by circles.

While the nuclear structure in the cold region can be studied by discrete spectroscopy, it becomes increasingly difficult in the region of damped motion where strong branching in the decay strength starts to dominate, to resolve the discrete transition; there are simply too many within the resolution bins, even when good 3-D data, with increased spatial resolution per band are available, as in the present case. However, as advocated earlier it is still possible to obtain information about the average properties of the damped rotational decay, by studying the fluctuations of counts in the experimental coincidence spectra of 1-, 2- or 3 dimensions, or by a careful study of the spectrum shapes, and compare the observations to simulation calculations as described above. The fluctuation analysis method for example, allows to obtain the effective number of decay paths which pass through specific parts of the spectrum. Since the transition energies in regular rotational bands are strongly correlated, they show up as characteristic patterns in the coincidence spectra displaying regular ridge structures along a diagonal valley for $E_{\gamma_1} = E_{\gamma_2}$. The valley on the other hand has lower intensity, because no transitions in a regular rotational band are equal. Therefore, transitions from the quasi-continuum can, with some care taken against "backbends" and "scars" showing up as peaks, be rather cleanly observed in the valley.

The selection of $E_{\gamma 1} \cdot E_{\gamma 2}$ coincidence spectra associated with some rather clean transitions belonging to specific configurations was made, as shown in the illustrative example in Fig. 7. It was possible on the GA.SP data to select seven γ-γ-spectra, one for each of the configurations (π, α) and one for each high-K bands.

The effective number of paths is shown [2, 3] most simply to be related to the fluctuations in the spectrum by the equation:

$$N^{(2)}_{\text{path}} = \frac{N_{eve}}{\frac{\mu_2}{\mu_1} - 1} \frac{P^{(2)}}{P^{(1)}}, \tag{1}$$

where μ_1 and μ_2 are the first and second moment of the number of counts in a sector of the $\gamma - \gamma$ matrix containing the number of events N_{eve}. The size of the sector must typically be $\frac{4}{\mathcal{J}} \times \frac{4}{\mathcal{J}}$, corresponding to 60 keV $\times$ 60 keV for rare earth nuclei, in order to have in average one count for each cascade. The factor $\frac{P^{(2)}}{P^{(1)}}$ is a correction due to the finite resolution of the detector system, defined through the relation:

$$P_j^{(n)} = \int (P_j(E))^n dE / \int dE. \tag{2}$$

It takes care of the fact that for a given path of energy E there is a certain probability $P_j(E)$ for detection in a channel j of the γ-γ spectrum. The second moment μ_2 is extracted relative to the average surface obtained in each point with the best fit of a third order polynomial to the 7×7 surrounding channels.

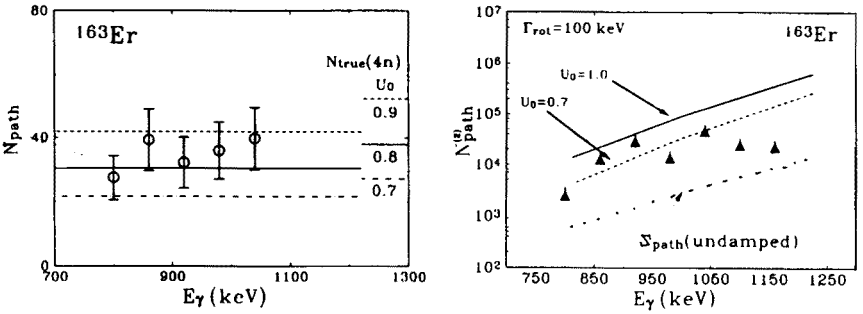

Fig. 9. The quantity $N^{(2)}_{\mathbf{path}}$ extracted from the valley in shown in the right part of the figure as a function of the γ-transition energy. Theoretical predictions of $N^{(2)}_{\mathbf{path}}$ are also shown. The dotted line is obtained summing over bands from U_0 up to ∞ without considering the damping of the rotational motion, and is in one order of magnitude lower than the data. The dashed and solid line are calculated including the rotational damping, with $\Gamma_{\mathrm{rot}} = 100$ keV and two different parametrizations of U_0. In the left part of the figure $N^{(2)}_{\mathbf{path}}$ extracted from the first ridge is shown. The experimental values are in agreement with the calculations where U_0 is between 0.8 and 0.9 MeV.

By making use of equation (1) the number of paths $N^{(2)}_{\mathbf{path}}$ populating the ridges has been extracted for ^{163}Er by integrating the ridge structure in corresponding μ_1 and μ_2 spectra. Typical values extracted for the high spin region are $N^{(2)}_{\mathbf{path}} \approx 35$ (see left part of Fig. 9). These results are typical for the rare earth region and demonstrate that the rotational pattern displaying a ridge structures originates from a cold nucleus, with low level density. For these regular discrete rotational bands, the paths at a given average transition energy E_γ consist of transitions along the bands from spin I to spin $I-2$, with $E_\gamma \approx (2\hbar^2/\mathcal{J}) \cdot I$; therefore $N^{(2)}_{\mathbf{path}}$ will give the number of bands below the energy $\mathrm{U_0}$, where the damping sets in, with a small correction for feeding $\mathrm{N_{true}/N_{path}}$ indicated in the left part of the figure. Integrating the level density up to different values of U_0, one obtains the corrected lines displayed in Fig. 9. One finds that the measured effective number of discrete bands 35, corresponds to $U_0 \approx 800$ keV, and that the true number of bands below U_0 is ≈ 40, or in other words, 10 in average for each parity and signature.

For the valley region, the number of paths determined through equation (1) is much higher, of the order of 10^4, as shown in the right part of Fig. 9. If the counts in the valley were produced by transitions along undamped bands with wildly fluctuating moments of inertia one could still obtain a theoretical estimate of $N_{\rm path}^{(2)}$ by summing over all bands from U_0 up to ∞. This gives the dotted curve (marked undamped), which for all nuclei is at least an order of magnitude smaller than the experimental values. The solid and dashed curves have on the contrary been obtained assuming damping of the rotational motion, with a damping width $\Gamma_{\rm rot} \approx 100$ keV, which is seen to reproduce the observations quite well.

The existence of two discrete deformation aligned bands both with K=19/2 at rather high excitation energy above yrast was previously known, [18] and shown in Fig. 8 as K1, K2. They can be well described by means of a "tilted axis cranking (TAC) model", by cranking about an axis tilted relative to the principal axes of the deformed potential [19] instead of the usual principal axis cranking (PAC). A third high-K band has been added recently (labeled K4 in Fig. 8) to the level scheme [20]. As one can see from Fig. 8, the high-K bands have an excitation energy varying between 0.8 and 1.4 MeV above yrast, the region where the rotational damping is expected to play an important role. However, the high-K bands are still good discrete rotational bands, which stand out from the underlying quasi-continuum states. The known decay out from these bands goes through the band head of the $[505]11/2^-$ configuration which is isomeric with a half-life of 0.58 μs.

Very clean γ-γ spectra were built for both the high-K (K1, K2 and K4) and the low K (yrast and other excited normal rotational bands) configurations. A ridge-valley structure is still present in the spectra in coincidence with high-K bands, but the rather smooth distribution of counts seems to vanish, in favor of larger fluctuations (see Fig. 7). Therefore the number of paths associated to these high-K configurations has to be different from those associated with the yrast band. A preliminary analysis of the co-variance between the high-K and low-K gated spectra shows very small overlap and supports this conclusion.

The number of paths in the valley for all the selected configurations is shown in the right part of Fig. 10 as a function of the gamma transition energy. As one can see, the number of paths increases with the γ-transition energy with about the same trends both for the yrast configuration and the other normal low-K bands, while it is roughly constant for the high-K bands. Moreover, the K1, K2 and K4 bands, lying approximately 1 MeV above the yrast, are fed by a number of paths that is an order of magnitude smaller than that associated with the normal configurations. In addition, the number of paths for the high-K bands becomes smaller as the excitation

energy above yrast increases, in contrast to the normal configurations, where the number of paths seems independent of the excitation energy, although the data is spanning over a region of 300 keV (see also Fig. 8).

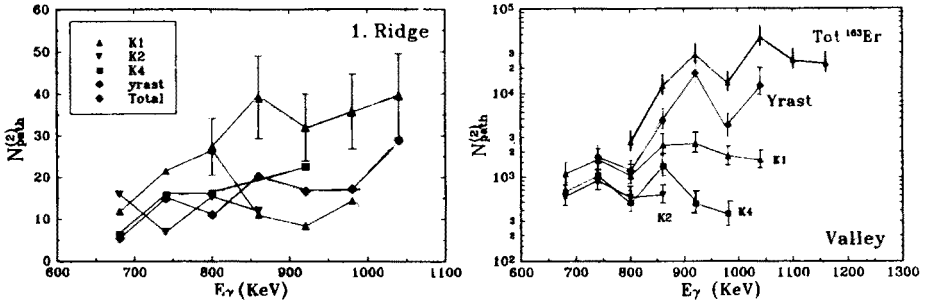

Fig. 10. The quantity $N^{(2)}_{path}$ extracted for the valley for each selected configuration is plotted in the right part of the figure as a function of the γ-transition energy. The solid lines connect the points to guide the eye only. The values for the yrast are plotted as representative for the low K configurations, but the same trends have been obtained for the other normal rotational bands. In the left part the $N^{(2)}_{path}$ extracted from the first ridge is shown for different configurations as labeled in the legend.

This is a clear indication that the mixing of states in the quasi-continuum, from where the feeding of the high-K bands originate, and presumably responsible for rotational damping in the case of high-K bands, is completely different and most probably decoupled from the normal states at the same energy. The difference could be attributed either to a particular feeding mechanism or to a persistent selectivity for the K quantum number at higher temperatures, although maybe not as stringent as the well known K-selection rules for the cold region along the yrast line.

The results of the analysis for the first ridge of different configurations are shown in the left part of Fig. 10. Here the number of paths corresponds to the number of regular rotational bands in coincidence with each selected configuration. Preliminary, the average number of paths was found to be $\approx$ 10–15, both for low and high-K bands. This result implies that there are in average 10–15 rotational bands associated with each type of configuration (K, π, α). This may not be so surprising, and implies that each of the configuration types are fed from only the damped region by statistical E1's, or from similar bands (fractionated to some degree) of the same type of configuration, namely those which they can be mixed with, yet obeying the standard selection rules. This conjecture also agrees with the fact that the total number of path for the 4 types (π, α) of low-K configurations was found to be 40, as shown in Fig. 2.

4. Scars of rotational bands, in the damped region

Several attempts have been made to measure the rotational damping width Γ_{rot} , most recently by use of the so-called Rotational Mapping Method, [21]. In this work the overall spectrum shape was analyzed on the basis of the assumptions given in the damping model of Lauritzen *et. al.* [1], namely that the transition energies at a given angular momentum were selected from the $B(E2)$ strength function independently of the preceding transitions in the same cascade, which may be characterized as *uncorrelated damping*. This implies that the 2-D coincidence spectrum is characterized by a valley along the $E_{\gamma_1} = E_{\gamma_2}$ diagonal, with a width and a depth which can be related to the rotational damping width $\Gamma_{\rm rot}$, as illustrated by the simple simulation calculations of Figs 11a, 11b, 11d and 11e.

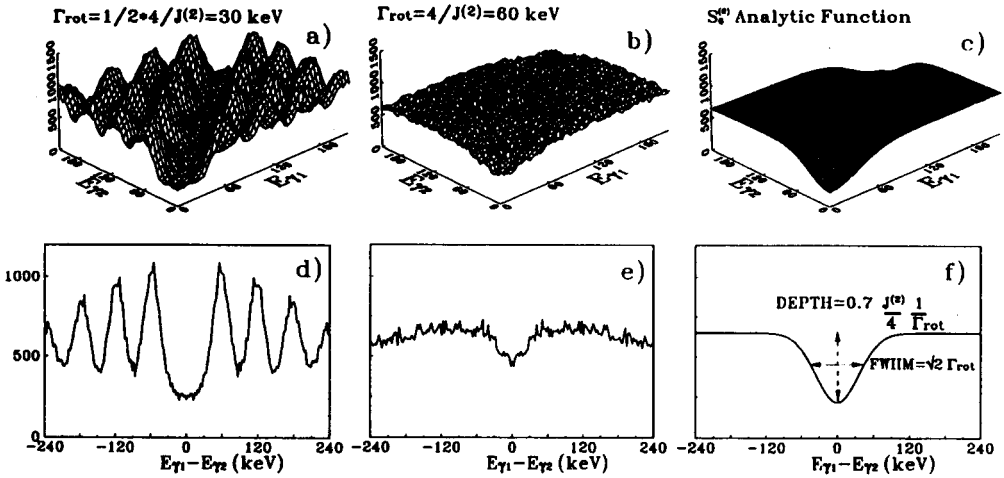

Fig. 11. $E_{\gamma 1} \cdot E_{\gamma 2}$ coincidence spectra produced by simple simulation calculations of 100000 damped nuclear γ-ray cascades are shown in part a) and b). The damping width values $\Gamma_{\rm rot} = 30$, 60 keV and constant moment of inertia $\mathcal{J}^{(2)} = 70$ MeV^{-1} have been used. Perpendicular cuts across the $E_{\gamma_1} = E_{\gamma_2}$ diagonal and 60 keV wide are given in part d) and e). The round hills obtained using $\Gamma_{\rm rot} = 30$ keV are completely smeared out for $\Gamma_{\rm rot} = 60$ keV, and only a very shallow valley survives. This suggests that, in the limit of $\Gamma_{\rm rot} \geq 4/\mathcal{J}^{(2)}$, the spectrum can be reproduced by the analytical function shown in part c) and f).

A set of analytical expressions was developed [22] and used to reproduce the distributions of the coincidence events in 2-D as well as 3-D spectra, assuming $B(E2)$ strength functions of either Gaussian or Breit–Wigner forms. These are the two different shapes expected theoretically for the $B(E2)$ distribution in the limit of low and high level density [1]. In particular, if the simple picture of *uncorrelated damping* is fulfilled, both the FWHM and

the DEPTH of the valley must be strictly related to $\Gamma_{\rm rot}$, giving a direct measure of the rotational damping width $\Gamma_{\rm rot}$, as shown in the example in Fig. 11c and 11f for 2-D coincidence spectra.

The method was used to analyze the two different nuclei ^{163}Tm [5] and ^{168}Yb [21]. Very high intensity data-sets were produced by both the NORDBALL, at NBI and EUROGAM I, at Daresbury, using the reactions ^{130}Te(^{37}Cl, xn)^{162,163}Tm, with $E_{\rm beam}$ = 166 MeV, and ^{124}Sn (^{48}Ca, xn)^{167,168}Yb, with $E_{\rm beam}$ = 210 MeV, respectively. The number of collected multi-fold events in the two experiments correspond to 8 $\times 10^8$ and 3 $\times$ 10^9 unfolded triple coincidences, respectively. The results obtained using the simple analysis for the two nuclei clearly indicate that the given relations between the measured width and depth of the "central valley" are not satisfied [5]. Moreover, the results deduced from the width alone yield $\Gamma_{\rm rot} \approx$ 80–100 keV, a factor of 2–3 lower than expected theoretically ($\Gamma_{\rm rot} \approx$ 250–300 keV) for $I \geq 40$. This strongly suggests that the picture of *uncorrelated damping* is too simple.

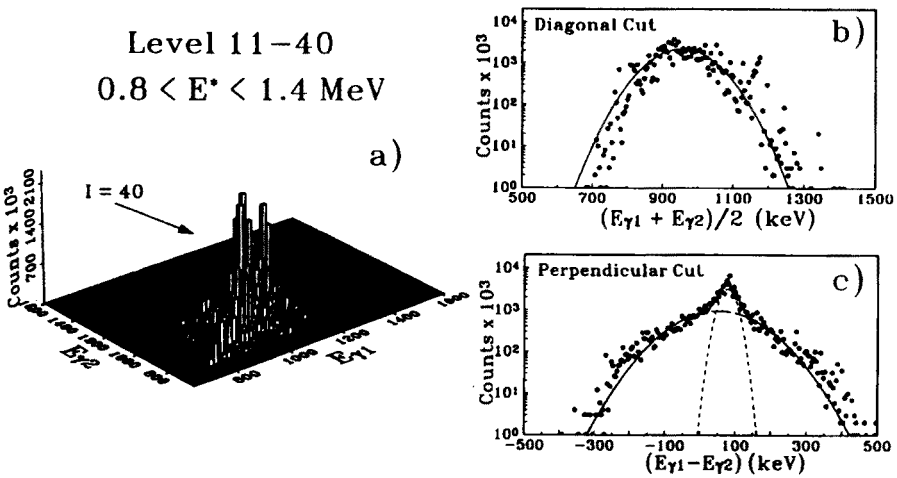

Fig. 12. The rotational correlations predicted by the band mixing calculations [10] are shown in the 2-D plot for the angular momenta sequence 42 → 40 → 38 for the group of levels 11–40 of ^{168}Yb, corresponding to the excitation energy region 0.8 $\leq E^* \leq$ 1.4 MeV, summing up the 4(π, α) configurations. Figure b) and c) show the projections on the $(E_{\gamma_1}+E_{\gamma_2})/2$ and $(E_{\gamma_1}-E_{\gamma_2})$ axis, respectively. As one can see, a strong correlation between the two transition energies can be observed in the difference as a narrow component, but not in the sum.

The assumptions underlying the damping model have been investigated microscopically by performing cranking and band mixing calculations for the high spin region ($30 < I < 60\hbar$) without pairing, but taking the full surface delta two-body residual interaction, [8] between all the states of same parity

and signature into account, as discussed earlier. It turns out that at least for the lowest 200 bands of each (π, α), which extends up to $\approx$ 2 MeV of excitation energy well into the damping region, the band mixing calculations predict significant rotational correlations in the subsequent steps of the cascade. This is illustrated in Fig. 12, for the lowest 40 bands (see also Fig. 6). The 2-D plot shows the coincidence pattern obtained selecting only 2 steps of the rotational decay with an angular momenta sequence $42 \rightarrow 40 \rightarrow 38$ for the levels 11–40, counted from yrast and summing up all the 4 parity-signature configurations of ^{168}Yb.

While the diagonal cut $(E_{\gamma_1} + E_{\gamma_2})/2$ of the 2-D pattern (Fig. 12b) shows, how the average energy of the two transitions is spread over a large energy interval, in accordance with the damping picture, the perpendicular projection $(E_{\gamma_1} - E_{\gamma_2})$ shows the existence of two components of nearly Gaussian shapes, centered around the energy expected for the ridge. The intensity and the width of the wide and narrow components have been fitted using two independent Gaussian functions, as function of the excitation energy above yrast and for different values of spin. In general one observes that the wide component behaves as expected for damped transitions, having a FWHM$\approx$ 200 – 400 keV $\approx \sqrt{2}\Gamma_{\rm rot}$, while the FWHM of the narrow part is $\approx$ 50 – 80 keV. With increasing heat energy, the intensity of the narrow component decreases, and correspondingly the wide component grows. This is shown in the right part of Fig. 13 for $I = 40\hbar$. This latter observation, together with the fact that the narrow component seems to be mostly originating from strong correlations along subsequent steps of the damped cascade (see left part of Fig. 13), may suggest that a remnant

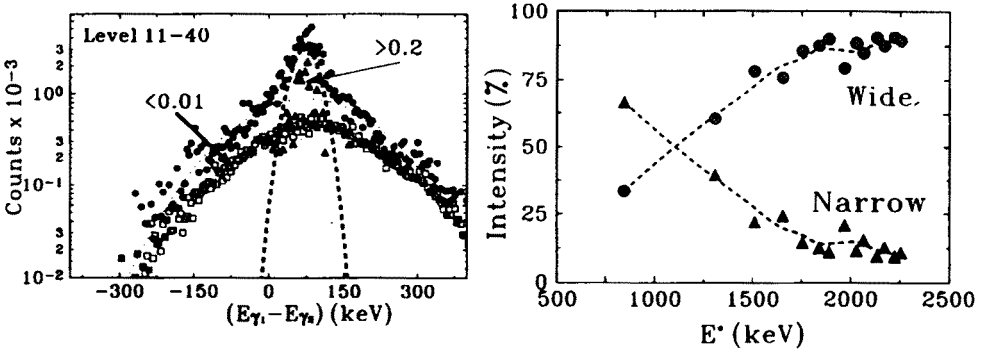

Fig. 13. The left side of the figure shows, for the group of level 11–40 at spin $I = 40\hbar$, the total ridge coming from γ-γ correlations (full circles), compared to the contribution from components with a probability larger then 0.2 (open triangles). Also shown is a sum of all the weak contributions smaller than 0.01. As one can see, the strongest correlations contribute mostly to the narrow part of the ridge. The intensity of the wide and narrow components at $I = 40\hbar$ are shown as function of excitation energy in the right part of the figure.

of rotational correlations extends higher up well into the damping region (*correlated damping*), before the rotational motion becomes fully damped.

These effects can also be traced in the experimental spectra, and new methods are being developed to be able to isolate the two components experimentally, and extract both the narrow and the wide component as a function of spin. The correlations can also be traced to a higher number of consecutive transitions, although the intensity decreases. On the other hand, rotational correlations are measured with higher sensitivity, in the rotational planes of a 3-D data-matrix, because the different ridges are selected according to the rotational relations among the transition energies

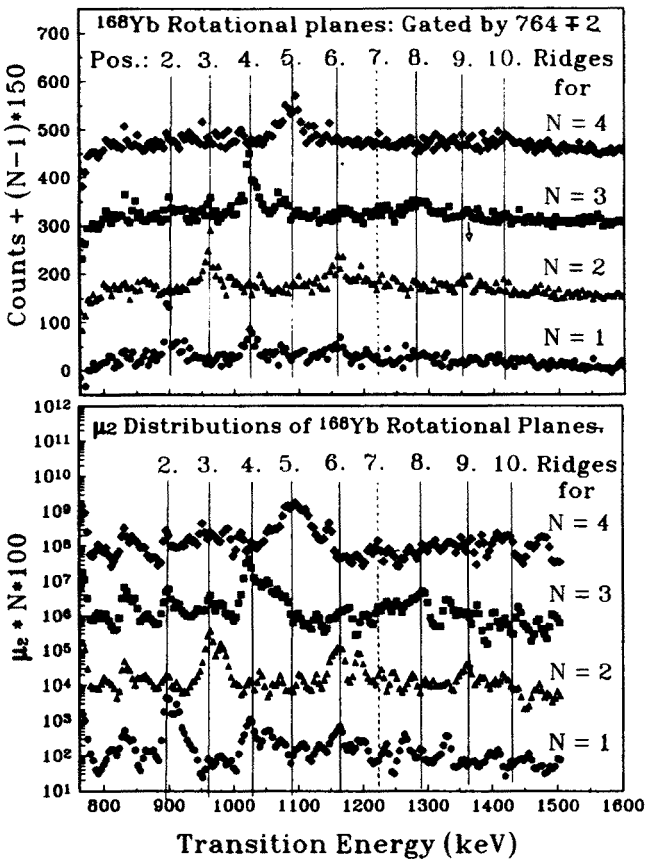

Fig. 14. The top part of the figure shows 4 spectra gated by 764±2 keV along stripes in $N = 1, 2, 3, 4$ rotational planes of a 3-D matrix of ^{168}Yb data. The corresponding μ_2/μ_1 spectra are shown in the lower part of the figure. The positions of the different ridge structures 2.-10. are indicated on the figure. In the $N = 1$ spectra ridges at position 2, 4, 6, 8 are only possible if the rotational patterns are obeyed, in contrast to position 3, 6, 9 for $N = 2$, and positions 4, 8 for $N = 3$ and 5, 10 for $N = 4$.

[21]. This is illustrated in Fig. 14, on data from the EUROGAM I experiment on ^{168}Yb discussed earlier [11]. The top part of the figure show 4 spectra gated by 764 $\pm$ 2 keV along stripes in N = 1, 2, 3, 4 rotational planes. The corresponding μ_2/μ_1 spectra are shown in the lower part of the figure. The positions of the different ridge structures 2–10 are indicated on the figure. In the N = 1 spectra ridges at position 2, 4, 6, 8 are possible, in contrast to position 3, 6, 9 for N = 2, and positions 4, 8 for N = 3 and 5, 10 for N = 4. It is evident that the expected patterns are seen both in the intensity spectrum, but even more so in the fluctuation spectra μ_2/μ_1 , where a logarithmic scale is used to increase the dynamic range. Note that the width of the gate is only 4 keV, but the rotationally correlated structures are 30–50 keV wide. The fact that the patterns are observed strongly in the μ_2/μ_1 spectra shows that the structures are made up of a low number of bands, $\leq$ 100 in agreement with expectations for the narrow component in the calculations. It therefore may be a result of the predicted *scars* of rotational motion, expected to be found at higher excitation energies. Further support for this conjecture is indicated by our most recent simulations based on inputs from the microscopic calculations [8], where similar structures can be observed both in the intensity and in μ_2/μ_1 spectra.

The work has been supported by the Danish Natural Science Research Council.

REFERENCES

[1] B. Lauritzen, T. Døssing, R.A. Broglia, *Nucl. Phys.*, **A457**, 61 (1986).

[2] B. Herskind, A. Bracco, R.A. Broglia, T. Døssing, A. Ikeda, S. Leoni, J. Lislie, M. Matsuo, E. Vigezzi, *Phys. Rev. Lett.*, **68**, 3008 (1992).

[3] T. Døssing, B. Herskind, S. Leoni, M. Matsuo, A. Bracco, R.A. Broglia, E. Vigezzi, *Phys. Rep.* (1995) to be published.

[4] T. Døssing, M. Matsuo, P. Bosetti, A. Bracco, S. Frattini, B. Herskind, S. Leoni, P. Rasmussen, E. Vigezzi, R.A. Broglia, to be published.

[5] S. Leoni, B. Herskind, T. Døssing, P. Rasmussen, P. Bosetti, A. Bracco, R. Broglia, S. Frattini, M. Matsuo, N. Nica, E. Vigezzi, A. Ataç, M. Bergström, A. Brockstedt, H. Carlssont, P. Ekströmt, F. Ingebretsen, H.J. Jensen, J. Jongman, G.B. Hagemann, R.M. Lieder, T. Lönnroth, A. Maj, B. Million, A. Nordlund, J. Nyberg, M. Piiparinen, H. Ryde, M. Sugawara, P.O. Tjøm, and A. Virtanen, *Nucl. Phys.* in press; see also: S. Leoni, T. Døssing, B. Herskind, P. Rasmussen, P. Bosetti, A. Bracco, S. Frattini, R. Broglia, E. Vigezzi, M. Matsuo, LBL-35687 (1994), p. 126.

[6] A. Bracco, S. Frattini, P. Bosetti, T. Døssing, B. Herskind, S. Leoni, M. Matsuo, E. Vigezzi, Proc. of the VII Int. Conf. on Nucl. Reactions Mechanism 1994, ed. E. Gadioli, to be published.

[7] E. Vigezzi, S. Frattini, P. Bosetti, A. Bracco, R.A. Broglia, T. Døssing,B. Herskind, S. Leoni, M. Matsuo, Proc. of the Workshop on Heavy Ion Fusion: Exploring the Varieties of Nucl. Properties, Padova, 1994, to be published.

[8] M. Matsuo, T. Døssing, B. Herskind, S. Frauendorf, *Nucl. Phys.* **564**, 345 (1993); M. Matsuo, T. Døssing, B. Herskind, S. Frauendorf, E. Vigezzi, R.A. Broglia, Proc. of the 21 INS symposium, Tokyo Oct 1992, *Nucl. Phys.* **A557**, 211c (1993).

[9] D.C. Radford, Proc. of Int. Seminar on the Frontiers of Nuclear Spectroscopy, Kyoto, Japan, Y. Yoshizawa, H. Kusakari and T. Otsuka, eds., World Scientific, Singapore 1993, p. 229-249.

[10] B. Herskind, T Døssing, N. Nica, S. Leoni, A. Bracco, R.A. Broglia, E. Vigezzi, M. Matsuo, Proc. of Int. Seminar on the Frontiers of Nuclear Spectroscopy, Kyoto, Japan, Y. Yoshizawa, H. Kusakari and T. Otsuka, eds., World Scientific, Singapore 1993, p. 17-52.

[11] A. Fitzpatrick, S.A. Araddad, R. Chapman, J. Copnell, F. Lind'en, J.C. Lisle, A.G. Smith, J.P. Sweeney, D.M. Thompson, W. Urban and S.J. Warburton, J. Simpson, C.W. Beausang, J.F. Sharpey-Shafer, S.J. Freeman, S. Leoni, and J. Wrzesinski, *Nucl. Phys.* **585**, 335 (1995).

[12] S. Leoni, Ph.D. Thesis, University of Milano, December 1992, to be published.

[13] B. Herskind, B. Lauritzen, K. Schiffer, R. A. Broglia, F. Barranco, M. Gallardo, J. Dudek, E. Vigezzi, *Phys. Rev. Lett.* **59**, 2416 (1987).

[14] K. Yosida, M. Matsuo, private communication, and to be published.

[15] I.M. Green, S.A. Mozkowski, *Phys. Rev.* **139**, B790 (1968); A. Faessler, *Fortschr. Phys.*, **16**, 309 (1968).

[16] R. Bark, G.B. Hagemann, B. Herskind, H.J. Jensen, W. Korten, M. Bergström, A. Brockstedt, H. Carlsson, A. Norlund, H. Ryde, P. Bosetti, S. Leoni, P. Tjøm and F. Ingebretsen, to be published.

[17] A. Nordlund, R. Bengtsson, P. Ekström, M. Bergström, A. Brockstedt, H. Carlsson, H. Ryde, Y. Sun, A. Atac, G.B. Hagemann, B. Herskind, H.J. Jensen, J. Jongman, S. Leoni, A. Maj, J. Nyberg, P.O. Tjøm, *Nucl. Phys.*, in press.

[18] A. Brockstedt, J. Lyttkens-Linden, M. Bergström, L.P. Ekström, H. Ryde, J. C. Bacelar, J. D. Garrett, G.B. Hagemann, B. Herskind, F.R. May, P.O. Tjøm, S. Frauendorf, *Nucl. Phys.* **A557**, 469 (1993).

[19] S. Frauendorf, *Nucl. Phys.* **A 557**, 259c (1993).

[20] P. Bosetti, A. Bracco, B. Herskind, S. Leoni, G.B. Hagemann, R.A. Bark, A. Brockstedt, P. Ekström, H. Carlsson, A. Nordlund, H. Ryde, F. Camera, S. Frattini, M. Mattiuzzi, B. Million, C. Rossi Alvarez, G. de Angelis, D. Bazzacco, S. Lunardi, M. de Poli, to be published.

[21] B. Herskind, T. Døssing, D. Jerrestam, K. Schiffer, S. Leoni J. Lislie, R. Chapman, F. Khazaie, J.N. Mo, *Phys. Lett.* **B276**, 4 (1992).

[22] P.H. Rasmussen, Master Thesis, University of Copenhagen, 1993.